Title

The glycan CA19-9 promotes pancreatitis and pancreatic cancer in mice.

Permalink

https://escholarship.org/uc/item/1pd630gb

Journal

Science (New York, N.Y.), 364(6446)

ISSN

0036-8075

Authors

Engle, Dannielle D
Tiriac, Hervé
Rivera, Keith D
et al.

Publication Date

2019-06-01

DOI

10.1126/science.aaw3145

Peer reviewed

RESEARCH ARTICLE

CANCER

The glycan CA19-9 promotes pancreatitis and pancreatic cancer in mice

Dannielle D. Engle[1,2]*, Hervé Tiriac[1,2]†, Keith D. Rivera[1], Arnaud Pommier[1,2]‡, Sean Whalen[3], Tobiloba E. Oni[1,2], Brinda Alagesan[1,2], Eun Jung Lee[1,2], Melissa A. Yao[1,2], Matthew S. Lucito[1,2], Benjamin Spielman[1,2], Brandon Da Silva[1,2], Christina Schoepfer[1,2], Kevin Wright[1,2], Brianna Creighton[1,2], Lauren Afinowicz[1,2], Kenneth H. Yu[4,5], Robert Grützmann[6], Daniela Aust[7], Phyllis A. Gimotty[8], Katherine S. Pollard[3,9], Ralph H. Hruban[10], Michael G. Goggins[10,11], Christian Pilarsky[6], Youngkyu Park[1,2], Darryl J. Pappin[1], Michael A. Hollingsworth[12], David A. Tuveson[1,2]§

Glycosylation alterations are indicative of tissue inflammation and neoplasia, but whether these alterations contribute to disease pathogenesis is largely unknown. To study the role of glycan changes in pancreatic disease, we inducibly expressed human fucosyltransferase 3 and β1,3-galactosyltransferase 5 in mice, reconstituting the glycan sialyl-Lewis[a], also known as carbohydrate antigen 19-9 (CA19-9). Notably, CA19-9 expression in mice resulted in rapid and severe pancreatitis with hyperactivation of epidermal growth factor receptor (EGFR) signaling. Mechanistically, CA19-9 modification of the matricellular protein fibulin-3 increased its interaction with EGFR, and blockade of fibulin-3, EGFR ligands, or CA19-9 prevented EGFR hyperactivation in organoids. CA19-9–mediated pancreatitis was reversible and could be suppressed with CA19-9 antibodies. CA19-9 also cooperated with the $Kras^{G12D}$ oncogene to produce aggressive pancreatic cancer. These findings implicate CA19-9 in the etiology of pancreatitis and pancreatic cancer and nominate CA19-9 as a therapeutic target.

Pancreatitis, or inflammation of the pancreas, is a painful, recurrent, and occasionally lethal medical disorder with limited treatment options. The incidence of acute and chronic pancreatitis is rising (1). Pancreatitis accounts for more than 275,000 hospitalizations in the United States per year, and the number of hospital admissions has increased by 20% over the past decade (2). The causes of pancreatitis include blockage of the pancreatic duct by gallstones, alcohol and certain drugs that cause acinar cell damage, medical procedures or trauma that damage pancreatic tissue, and autoimmune diseases (2). In approximately one-third of cases, the underlying etiology of the pancreatitis is unknown (idiopathic) (3, 4). Most acute pancreatitis cases will resolve with supportive care; however, up to 20% of patients will develop severe tissue damage and will either succumb to multiorgan system failure or suffer from bouts of recurrent disease with markedly diminished quality of life (2–4). Individuals with hereditary acute pancreatitis progress to chronic pancreatitis with a much higher penetrance and have a 40 to 55% lifetime risk of developing pancreatic cancer (1, 5). Indeed, chronic pancreatitis promotes mutant Kras-mediated development of pancreatic cancer in mice (6).

The glycan carbohydrate antigen 19-9 (CA19-9) is found in the serum of 10 to 30% of pancreatitis patients and in 75% of pancreatic cancer patients, as well as in patients with other gastrointestinal diseases (7–16). CA19-9 elevation is also detected in pancreatic intraepithelial neoplasms (PanINs), which are precursors to pancreatic ductal adenocarcinoma (PDAC) (17). CA19-9 [sialyl-Lewis[a] (sLe[a])] is generated by the stepwise addition of sugar moieties to type I precursor chains present on proteins and other molecules, culminating in the α1,4 linkage of fucose to N-acetylglucosamine (fig. S1A). Fucosyltransferase 3 (FUT3) is the only enzyme with the ability to add fucose moieties through an α1,4 linkage and generate CA19-9. Mice lack this enzyme because Fut3 is a pseudogene in rodents (18, 19).

To facilitate the discovery of PDAC biomarker candidates, we sought to create a mouse model of PDAC that recapitulated the elevation of CA19-9 observed in human patients. This model would enable prioritization of biomarkers that outperform CA19-9. Furthermore, changes to glycosylation often result in functional consequences. In this study, we investigated the role of CA19-9 elevation in mouse and organoid models of pancreatic disease.

Recapitulation of CA19-9 elevation and regulation in cultured mouse PDAC cells

To express CA19-9 in mouse cells, we transduced mouse PDAC cells with human FUT3. Expression of FUT3 alone was insufficient for CA19-9 production but did lead to increased levels of Lewis[x] antigens after removal of terminal galactose moieties present in rodents but not humans (Fig. 1A). The generation of the related Lewis[x] epitopes suggested that reprogramming of the precursor substrates would be necessary for the production of CA19-9 in pancreatic ductal cells. β1,3-galactosyltransferase 5 (β3GALT5) is required for the production of type I chain precursors (20), which serve as the precursors for the Lewis[a] modification (fig. S1A). Accordingly, expression of both FUT3 and β3GALT5 in mouse PDAC cells led to the cell surface expression of CA19-9 at levels equivalent to those observed in human cancer cell lines (COLO205, SUIT2) (Fig. 1B and fig. S1B). Comparable CA19-9 levels were observed in the blood of mice after orthotopic transplantation of the CA19-9–expressing mouse and human cells (fig. S1C).

To determine whether the murine PDAC cell proteins harboring CA19-9 modification are similar to those in human PDAC cells, CA19-9 protein carriers were immunoprecipitated (IP) and identified by mass spectrometry (MS) (fig. S2A and table S1). These analyses identified known CA19-9 protein carriers in the FUT3- and β3GALT5-expressing mouse cells (n = 3; FC1199, FC1242, FC1245), including CD44, LGALS3BP, MUC1, and MUC5AC (21–24). The human PDAC cell line, MiaPaCa-2, is CA19-9 negative, and therefore, we used it as a control to identify human CA19-9 core proteins in the CA19-9–positive cell lines, Capan-2, SUIT2, and hM1-2D (fig. S2B and table

S2). We compared mouse and human CA19-9 protein carriers and found that an average of 72.3% (95% confidence interval 60.3 to 84.3%; n = 3) of the CA19-9–modified proteins identified in all three human PDAC cell lines were also found in the engineered murine PDAC cell lines. Thus, expression of the human FUT3 and β3GALT5 genes in mouse cells largely recapitulates the human CA19-9 carrier profile (Fig. 1C).

CA19-9 elevation in mice leads to acute and chronic pancreatitis

We next generated a mouse model with inducible CA19-9 expression to study the effects of this glycan on pancreatic disease pathogenesis (fig. S2, C to E). Using PDX1-Cre (C), we restricted expression of the transgenes to the pancreas, duodenum, and bile duct. Cre-mediated excision of a LoxP-flanked stop (LSL) cassette enables ubiquitous expression of the reverse tetracycline-controlled transactivator 3 and mKate2 from the CAGS promoter within the ROSA26 locus (R^{LSL}) (25). Addition of doxycycline (Dox) to the diet activates the reverse tetracycline-controlled transactivator, enabling FUT3, β3GALT5, and enhanced green fluorescent protein (eGFP) expression from the tetracycline response element promoter in the COLA1 locus (F) (26). In addition, we excised the LSL cassette in the R allele to generate animals with Dox-inducible, whole-body CA19-9 expression (R;F). Both $C;R^{LSL};F$ and R;F Dox-treated mice exhibited histologic signs of pancreatitis, including interstitial edema, lymphocyte infiltration, and collagen deposition (Fig. 2A and fig. S3, A and B). All other nonpancreatic tissues appeared histologically normal in both Dox-treated and untreated models and their littermate controls (figs. S4 and S5). The mice progressed from acute to chronic pancreatitis after 28 days of Dox treatment as demonstrated by the clinical histopathological hallmarks of acinar atrophy, accumulation of metaplastic ductal lesions, and persistent fibroinflammatory disease (figs. S3, A and B, and S6, A and B) (27). Pancreatitis was highly penetrant in both models (Fig. 2B and fig. S6, C and D).

Both mouse models demonstrated elevated serum levels of the pancreatic enzymes amylase and lipase within 24 hours of Dox treatment, but no changes were observed in untreated mice and littermate controls (Fig. 2C and fig. S6, C and D). Patients with acute pancreatitis have elevated serum levels of amylase and lipase, but in the chronic phase of pancreatitis, the levels of these enzymes either normalize or decrease even further. We found in our mouse models that the levels of amylase and lipase began to normalize after 4 weeks of Dox treatment, but both $C;R^{LSL};F$ and R;F mice still exhibited histologic signs of chronic pancreatitis. Expression of eGFP and CA19-9 was detected in the pancreas after Dox treatment of $C;R^{LSL};F$ mice and R;F mice, but they were not detected in untreated or control littermates (Fig. 2A and figs. S3C, S7, and S8). In both mouse models, CA19-9 was predominantly expressed in intralobular, intercalated, and meta-

plastic pancreatic ducts as well as in islet cells (Fig. 2A and figs. S3C, S7, and S8). Both models exhibited elevated CA19-9 levels in the circulation (Fig. 2D and fig. S6, C and D). Secreted CA19-9 was also observed coating eGFP-negative endothelial cells as well as fibroblasts (figs. S7B and S8). E-selectin is an endogenous receptor of CA19-9 expressed by endothelial cells (28, 29) and may explain the accumulation of CA19-9 within the vasculature. Despite recombination in the acinar compartment, acinar cells were rarely observed to be CA19-9 positive. R;F mice exhibited Dox-dependent expression of CA19-9 and eGFP in all tissues examined, whereas in $C;R^{LSL};F$ mice, expression was limited to the pancreas, duodenum, and gall bladder (Fig. 2A and figs. S3, C to G, and S7 to S11).

We next sought to determine the prevalence of CA19-9 elevation in human pancreatic disease and to compare the CA19-9 tissue expression pattern observed in human patients and the CA19-9 genetically engineered mouse models. We therefore evaluated CA19-9 levels and expression patterns in patients, including specimens of pancreatic cancer and adjacent normal tissue (n = 72) as well as surgically resected chronic pancreatitis samples (n = 44) (figs. S12 and S13). CA19-9 was expressed at low levels in normal homeostatic pancreatic ducts and at elevated levels in adjacent reactive ducts that consist of atypical, benign pancreatic ducts that occur even in the absence of substantial inflammation (fig. S12A), preinvasive carcinomas (PanIN-1A and PanIN-1B), and invasive PDAC specimens (fig. S12, B to D) (17). In chronic pancreatitis specimens, CA19-9 was expressed at high levels in the reactive and metaplastic ducts with more sporadic expression in the centroacinar and acinar compartments (fig. S13, A and B, and table S3). Elevated levels of CA19-9 were detected in the serum of 20% of the chronic pancreatitis patients we examined, whereas more than 93% of these patients exhibited local elevation of CA19-9 in the resected pancreatic specimens by immunohistochemistry (IHC) (n = 44) (fig. S13, C and D). Together, these data indicate that CA19-9 elevation is a common feature of chronic pancreatitis and that the CA19-9 expression pattern is similar between the CA19-9 mouse models and human patients.

Patients with severe acute or chronic pancreatitis often also exhibit weight loss (30, 31). Therefore, we assessed the health and weight of both mouse models. Whereas most $C;R^{LSL};F$ mice maintained their overall health status after Dox treatment, Dox-treated R;F mice exhibited significant body weight loss (fig. S14A). In severe cases, the weight loss exceeded 20%, and euthanasia was required. The weight loss was not due to pathology of the stomach, duodenum, or colon and was not associated with an autoimmune reaction, induction of endoplasmic reticulum stress in the pancreas, or loss of glycemic control (32) (fig. S14, B to D). Pancreatic exocrine
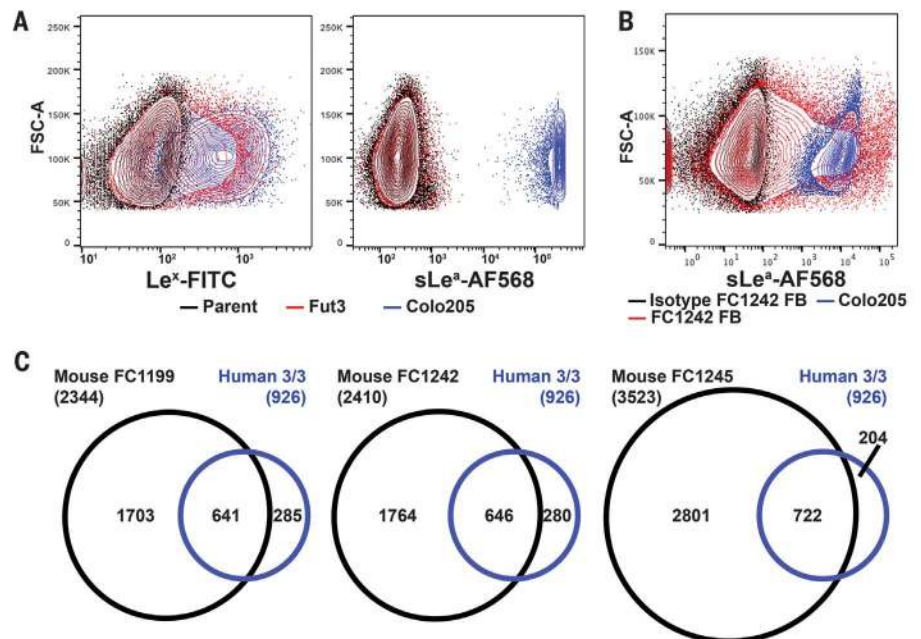

Fig. 1. FUT3 with β3GALT5 expression enables CA19-9 production in engineered mouse pancreatic cancer cells. (**A**) Ectopic FUT3 induces Lewis^x (Le^x) but not CA19-9–sLe^a expression in mouse PDAC cells by flow cytometric analysis. The Le^x- and CA19-9–sLe^a—positive human cell line COLO205 and Le^x- and CA19-9–sLe^a—negative parental KPC cell lines are shown. FITC, fluorescein isothiocyanate; FSC-A, forward scatter–area; AF568, Alexafluor 568. (**B**) CA19-9 flow cytometry of mouse PDAC cells stably and constitutively expressing FUT3 with β3GALT5 (FB) compared with the isotype control antibody. (**C**) Overlap between CA19-9 protein carriers identified in three out of three human PDAC cell lines (n = 926) with three independent mouse PDAC cell lines expressing FUT3 and β3GALT5.

insufficiency is often observed in cases of chronic pancreatitis and can cause severe weight loss and destruction of the acinar compartment in patients (*31*). R;F mice exhibited a significant Dox-dependent decrease in pancreatic mass, whereas no change was observed in C;R^LSL;F mice and littermate controls after Dox treatment (fig. S14E). In addition, we observed a significant and sustained increase in steatorrhea in R;F mice, whereas C;R^LSL;F mice exhibited a transient increase in fecal triglycerides that normalized within 4 weeks of Dox treatment (fig. S14F). The pancreatic atrophy and steatorrhea in R;F mice was accompanied by a significant reduction of fecal elastase in R;F mice within the first week of Dox treatment (fig. S14G). Together, these data indicate that R;F mice suffer from pancreatic atrophy and exocrine insufficiency. Both the increased penetrance of CA19-9 expression in the Cre-independent R;F model

and expression of CA19-9 in other tissues may contribute to the severe pancreatitis observed in this model.

Human pancreatitis is associated with an influx of macrophages to the pancreas during the acute phase of the disease; after progression to a chronic condition, T and B cells also infiltrate the pancreas (*33, 34*). To determine whether this aspect of human pancreatitis is also found in mouse models of pancreatitis, we examined the immune infiltrate in C;R^LSL;F mice and the established cerulein model of acute pancreatitis. Flow cytometry revealed an influx of immune cells into the pancreas, including recruitment of inflammatory monocytes and macrophages, after induction of pancreatitis (Fig. 2E and figs. S15 and S16A). This result was confirmed by IHC (fig. S16B). Neither model showed significant recruitment of T or B cells at the acute pancreatitis time points examined by flow cytometry (1 to

3 days) (fig. S15). At the chronic phase of pancreatitis, both R;F and C;R^LSL;F models contained intrapancreatic T and B cells as indicated by IHC (fig. S17). Therefore, both the CA19-9 and cerulein mouse models of pancreatitis exhibited immune infiltrates similar to those found in patients with pancreatitis.

Pancreatic cell proliferation is a common feature of human pancreatitis (*35*). Cerulein-treated mice exhibited an elevation in Ki67-positive nuclei in the infiltrating immune cells as well as in the ductal and acinar compartments. Similarly, both R;F and C;R^LSL;F mice exhibited increased Ki67-positive nuclei in the immune, acinar, and ductal compartments in the acute phases of pancreatitis, which gradually diminished as the mice progressed to chronic pancreatitis (fig. S18, A to E). Increased ethynyl deoxyuridine (EdU) incorporation was also observed in the pancreas, including elevation in the immune, ductal, and
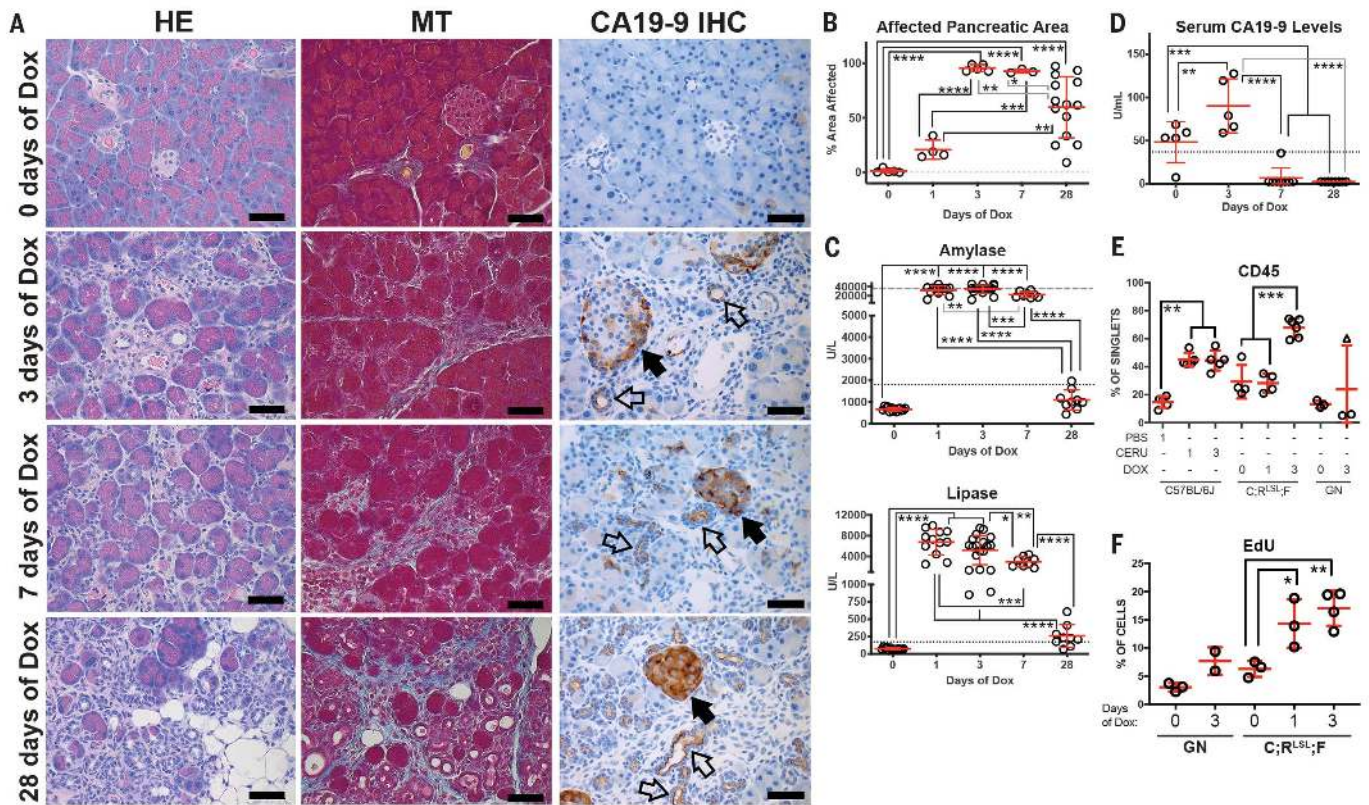

Fig. 2. CA19-9 expression promotes pancreatitis in mice. (**A**) Histologic evaluation of C;R^LSL;F mice by hematoxylin and eosin (HE) staining, Masson's trichrome staining (MT) (blue indicates collagen deposition), and CA19-9 expression (open arrow, CA19-9⁺ duct; closed arrow, CA19-9⁺ islet) by IHC after treatment with Dox. Scale bars = 50 μm. (**B**) Quantification of the percentage of pancreatic area exhibiting histologic signs of pancreatitis after treatment of C;R^LSL;F mice with Dox. (**C**) Circulating levels (U/L) of the pancreatic enzymes amylase and lipase in C;R^LSL;F mice after treatment with Dox (days). The dotted line indicates the threshold elevation required for the diagnosis of pancreatitis. The dashed line indicates the maximum level of detection possible for amylase. (**D**) The circulating level of CA19-9 (U/ml) after treatment of C;R^LSL;F mice with Dox. Values that exceed 37 U/ml (dotted line) are elevated. (**E**) Immune cell infiltration evaluated by flow cytometry

in mice treated with phosphate-buffered saline (PBS) or cerulein (Ceru) for 2 days followed by a 1- or 3-day recovery period (C57Bl/6j; n = 5, 5, and 5, respectively) and C;R^LSL;F mice treated with Dox (n = 4, 4, and 6, respectively) compared with "genetically negative" controls (GN) (n = 3 and 3, respectively). Outlier analysis using Grubb's method identified one data point (triangle symbol, GN, 3 days of Dox) as an outlier. (**F**) EdU incorporation in the pancreas was evaluated by flow cytometry in C;R^LSL;F mice (n = 3, 3, and 4, respectively) and littermate GNs (n = 3 and 2, respectively) after treatment with Dox. Middle horizontal red lines represent the mean, and error bars represent the standard deviation; each data point represents a measurement from an individual mouse. *P < 0.05, **P < 0.01, ***P < 0.001, ****P < 0.0001 for multiple comparisons using Holm-Sidak's procedure following a one-way analysis of variance.

fibroblast compartments (Fig. 2F and fig. S18F). Together, these data demonstrate that CA19-9–mediated pancreatitis in mice bears similarity to the human disease.

CA19-9 expression results in hyperactivation of epidermal growth factor receptor signaling

To identify the molecular mechanisms underlying the pancreatitis phenotype observed in mice, we focused our studies on the C;R^{LSL};F model. Other researchers have established that epidermal growth factor receptor (EGFR) signaling is necessary and sufficient for the induction of pancreatitis and is important for the initiation of pancreatic cancer in mice (36, 37). Accordingly, we found that the levels of tyrosine phosphorylated and activated EGFR were prominently elevated in the pancreatic ducts of C;R^{LSL};F mice after Dox treatment (Fig. 3A). To identify the alterations in cell signaling pathways that occur in direct response to CA19-9 expression, we isolated pancreatic ductal organoids from C;R^{LSL};F mice (38). RNA-sequencing analyses of the C;R^{LSL};F organoids after induction of CA19-9 expression revealed the expected changes in transgene expression (fig. S19, A to F, and table S4). FUT3 and β3GALT5 expression levels were comparable between mouse and human ductal organoids (fig. S19D) (39).

Gene set enrichment analysis identified significant changes to 21 pathways in the hallmarks of cancer gene sets and 64 pathways annotated in the KEGG (Kyoto Encyclopedia of Genes and Genomes) pathway gene sets (Fig. 3B and table S4). CA19-9 expression triggered a reduction in expression of genes associated with the unfolded protein response and an increase in expression of genes associated with chemokine, hedgehog, Janus kinase–signal transducers and activators of transcription, and transforming growth factor–β signaling. The latter genes may participate in the activation of the fibroblast compartment and recruitment of the immune infiltrate (e.g., interleukin-1a, colony-stimulating factor 1, tumor necrosis factor). We further explored enrichment of the extracellular matrix (ECM)–receptor interaction, ERBB, phosphatidylinositol 3-kinase (PI3K), and AKT signaling pathways (Fig. 3B). CA19-9 expression in C;R^{LSL};F organoids resulted in elevated EGFR phosphorylation (Y1068 and Y1148) and decreased total EGFR, indicating greater flux through this pathway (40) (Fig. 3C and fig. S20, A, B, and E to G). The increase in phosphorylated EGFR was accompanied by increased phosphorylation of focal adhesion kinase (FAK) (Y397), AKT, and extracellular signal–regulated kinase 1 and 2 (ERK1/2) (Fig. 3C and fig. S20F). Coincident FAK and EGFR activation through integrin-mediated interaction with the ECM has been previously reported in three-dimensional but not monolayer culture models (41, 42). EGFR stimulation by EGF was more rapid and robust in organoids that were previously cultured in EGF-free conditions, but EGF stimulation did not ind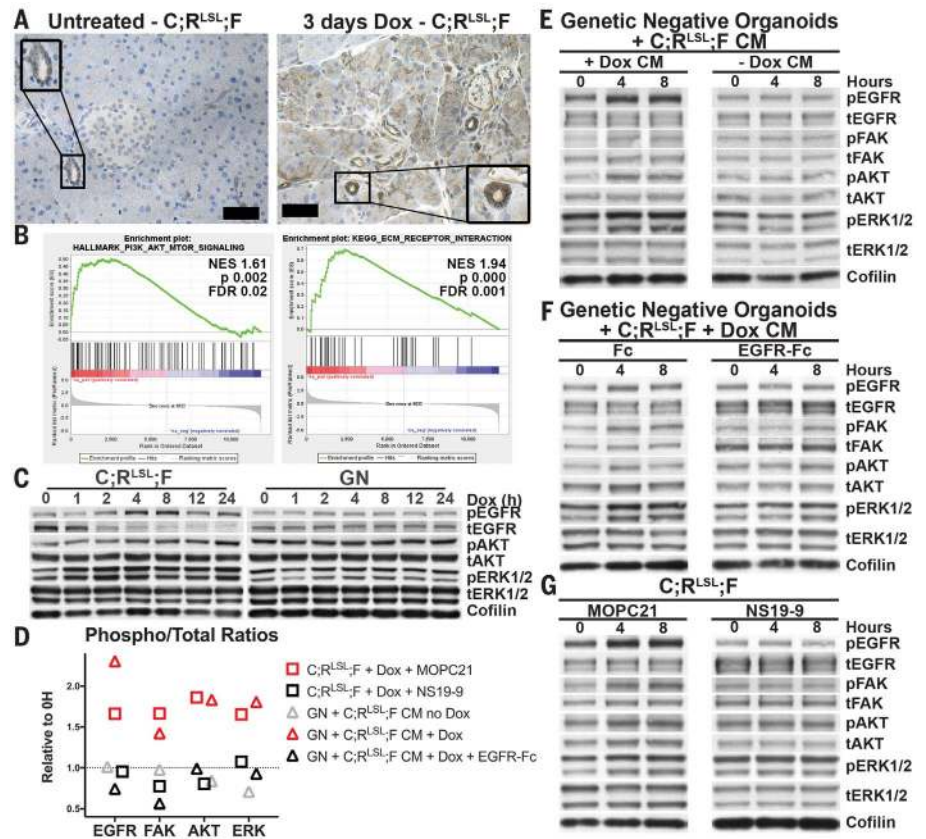uce FAK phosphorylation (fig. S20, C and D). Although the alterations of phosphorylated EGFR, total EGFR, and their ratio were consistent among biological replicates, no consistent changes to total or phosphorylated S6, HER2, and p65 were observed (fig. S20, A and B). These findings were independent of the inclusion of murine EGF in the media of the cultures (fig. S20E), and the level of phospho- and total EGFR and downstream effector induction exceeded the increase observed after treatment with additional EGF (fig. S20, B to D).

The glycosylation state of EGFR has been reported to affect its ability to activate and to respond to targeted kinase inhibitors (43, 44). Accordingly, we examined whether EGFR was modified by CA19-9 in mouse organoids, but this was not detected (fig. S20H). To investigate whether the CA19-9–dependent activation of EGFR was due to a soluble ligand, we evaluated conditioned medium from CA19-9–expressing organoids and found that it stimulated EGFR phosphorylation in control murine ductal organoids (Fig. 3, D to F). This activity was attenuated by the addition of EGFR-Fc (EGF trap), further supporting the presence of one or more EGFR ligands (Fig. 3, D and F). Addition of a monoclonal antibody to CA19-9 (NS19-9) was also sufficient to block EGFR phosphorylation in C;R^{LSL};F organoids (Fig. 3, D and G). These findings suggested the presence of a CA19-9–modified, secreted EGFR ligand.

EGFR complexes from C;R^{LSL};F organoid lysates were identified by IP-MS (Fig. 4A and table S5). We observed elevated levels of endogenous fibulin-3 [Efemp1 (FBLN3)] by IP-MS in C;R^{LSL};F, but not control organoids, after Dox treatment (Fig. 4A). FBLN3, a secreted matricellular glycoprotein with five EGF-like domains,

Fig. 3. CA19-9 expression activates EGFR signaling. (**A**) Representative phosphorylated EGFR IHC in C;R^{LSL};F mice that were treated for 0 ($n = 4$) or 3 ($n = 5$) days with Dox. Insets are higher magnification of pancreatic ducts. Scale bars = 50 μm. (**B**) Gene Set Enrichment Analysis of C;R^{LSL};F organoids identified enrichment in PI3K/AKT/mTOR and ECM-receptor signaling and downstream effector pathways. FDR, false discovery rate; NES, normalized enrichment score. (**C**) C;R^{LSL};F organoids ($n = 3$ biological replicates) and GN organoids ($n = 2$ biological replicates) were evaluated by immunoblot for the activation of signaling pathways after treatment with Dox. Blots are representative of three technical replicates, three biological replicates of C;R^{LSL};F organoids, and two biological replicates of GN organoids. p, phosphorylated; t, total. (**D**) Quantification of changes to the ratio of phosphorylated to total protein is shown for Fig. 3, E to G. (**E** and **F**) Organoids from GN littermates were incubated with conditioned media (CM) from C;R^{LSL};F organoids with or without previous Dox treatment (24 hours) in the presence or absence of Fc control or EGFR-conjugated Fc and evaluated by immunoblot. (**G**) C;R^{LSL};F organoids ($n = 3$ biological replicates) were treated with Dox (hours) in the presence of isotype control (MOPC-21) or CA19-9–blocking monoclonal antibody (NS19-9) and evaluated by immunoblot. Blots are representative of two technical and three biological replicates.

has been proposed to be a ligand for EGFR (*45*). Furthermore, we performed CA19-9 IP-MS from the conditioned media using two different CA19-9 monoclonal antibody clones and identified FBLN3 as a secreted, CA19-9–modified protein (Fig. 4B, fig. S21A, and table S6).

To confirm the glycosylation status of FBLN3, we coexpressed FLAG epitope–tagged FBLN3 in the presence or absence of FUT3 and β3GALT5 in mouse PDAC cells and detected CA19-9 modi-

fication of secreted FBLN3 (fig. S21B). The mRNA expression of fibulin family members and EGFR ligands did not change after Dox treatment of C;R^{LSL};F organoids (fig. S21C). Furthermore, the total protein levels of FBLN3 were unchanged after CA19-9 expression in organoid-conditioned media and in mouse plasma in vivo (fig. S21D). Secreted FLAG-FBLN3 isolated by immunoprecipitation coprecipitated with EGFR in PDAC cell lysates, consistent with an association of

FBLN3 with EGFR (Fig. 4C). Because the association of ectopic FLAG-FBLN3 with EGFR in cell lysates occurs irrespective of its CA19-9 glycosylation status, the finding that the glycosylation status of endogenous FBLN3 increases association with EGFR may reflect the interaction of sLe^a–modified FBLN3 with additional extracellular proteins. To determine whether FBLN3 is necessary for the activation of the EGFR pathway after CA19-9 expression, multiple FBLN3-blocking antibodies and short-hairpin RNA (shRNA) vectors were utilized and shown to prevent EGFR phosphorylation and the activation of downstream effector pathways in C;R^{LSL};F organoids (Fig. 4, D and E, and fig. S21, E and F).

CA19-9 as a therapeutic target in pancreatitis

We designed a Dox pulse-chase approach to determine if CA19-9 expression is required to maintain pancreatitis. CA19-9–mediated pancreatitis was completely reversed in C;R^{LSL};F mice after a 3-day Dox pulse and 4-day recovery period (fig. S22, A to C). Partial resolution of chronic pancreatitis in the C;R^{LSL};F model (28-day Dox treatment) was also observed after a 14-day recovery period (fig. S22, D and E). In a preventive setting of acute pancreatitis, two antibodies directed against CA19-9 both reduced immune infiltration, ductal metaplasia, and fibrosis in vivo (Fig. 5A and fig. S22, F and G). In addition, decreased release of amylase and lipase into the circulation and reduced hyperactivation of EGFR were observed (Fig. 5, B and C, and fig. S22, H and I). In an intervention setting of existing acute pancreatitis, we found that two forms of 5B1 significantly reduced the secretion of amylase into the circulation with modest normalization of the pancreatic histology (fig. S22, J to L). CA19-9 antibody treatment of existing acute pancreatitis also reduced the levels of phosphorylated EGFR in both the ductal and acinar compartments and decreased recruitment of macrophages (fig. S22, M and N). These data suggest that CA19-9 plays a role in disease pathogenesis and maintenance and that CA19-9–targeted therapy may warrant further therapeutic exploration.

Inhibition of EGFR in vivo by using erlotinib was not as effective as CA19-9 antibody blockade to mitigate pancreatitis induction in mice (fig. S23, A to F). Indeed, erlotinib treatment of CA19-9–expressing mice caused severe weight loss, necessitating euthanasia. These effects were unrelated to erlotinib toxicity in control mice. Although serum levels of amylase and lipase decreased in erlotinib-treated animals, pancreatic atrophy and acinar cell vacuolization were observed, suggesting that the weight loss were due to increased pancreatitis severity and resulting exocrine insufficiency (fig. S23, B and C). Erlotinib treatment also incompletely blocked phospho-EGFR levels in vivo (fig. S22D). Acinar-ductal metaplasia (ADM) can be detected by SOX9 IHC (*36*) and occurred after 7 days of Dox treatment in the C;R^{LSL};F model (fig. S22E). Although ADM was less apparent in the erlotinib-treated
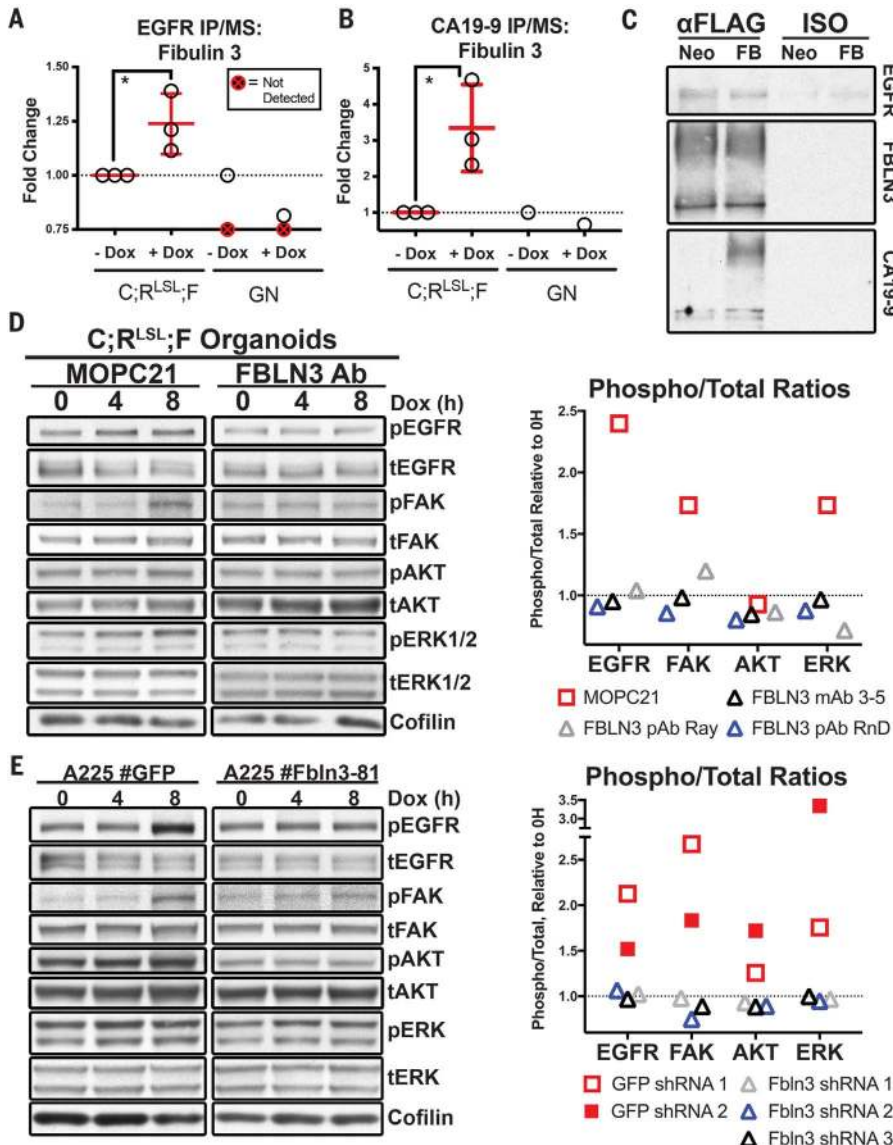

Fig. 4. CA19-9–modified fibulin-3 activates EGFR. (**A**) IP-MS of EGFR complexes from C;R^{LSL};F (*n* = 3) and GN organoid (*n* = 2) whole-cell lysates after Dox administration (8 hours). (**B**) CA19-9 protein carrier IP-MS analysis of fibulin-3 from conditioned media from C;R^{LSL};F organoids treated with Dox for 0 to 8 hours (*n* = 3) relative to untreated and treated GN organoids (*n* = 1) using 5B1 CA19-9 antibody clone. (**C**) Immunoblot of IP fibulin-3 (FLAG) after incubation with lysates from pancreatic cancer cells lacking FLAG-FBLN3 expression. ISO, isotype control antibody. (**D**) C;R^{LSL};F organoids (*n* = 3) treated with Dox in the presence of MOPC-21 or three independent fibulin-3 antibodies (FBLN3 Ab) and evaluated by immunoblot. Changes to the ratio of phosphorylated to total protein levels are included. mAb, monoclonal antibody; pAb, polyclonal antibody. (**E**) Organoids transduced with hairpins to GFP or to FBLN3 were immunoblotted after Dox treatment. Changes to the ratio of phosphorylated to total protein levels are included. Middle horizontal red lines represent the mean, and error bars represent the standard deviation. *P < 0.05 by unpaired, two-tailed *t* test.

C;R^{LSL};F mice (fig. S22F), lymphocyte infiltration and fibrosis remained unaffected. CA19-9 sequestration is unlikely to interfere with ADM survival mechanisms in the acinar compartment, given that these cells are largely CA19-9 negative (46). Therefore, EGFR kinase inhibition alone cannot substitute for CA19-9 blockade and may be a harmful therapy in the setting of pancreatitis.

Pancreatic tumorigenesis is accelerated by CA19-9–mediated pancreatitis

To determine whether CA19-9 expression promoted PDAC, we intercrossed the C;R^{LSL};F alleles with the conditional Kras$^{LSL-G12D}$ allele (K;C;R^{LSL};F) (fig. S24A) (47, 48). CA19-9 expression significantly accelerated pancreatic cancer lethality relative to untreated mice and control littermates (Fig. 6A). When treated with Dox, K;C;R^{LSL};F mice rapidly succumbed to primary and metastatic pancreatic cancer with a median survival of 202 days relative to 460 days in the K;C control cohort and 420 days in the untreated K;C;R^{LSL};F cohort. The primary tumors were anaplastic with glandular features (Fig. 6B). Widespread metastases were observed in the peritoneum, diaphragm, liver, and lung in multiple Dox-treated K;C;R^{LSL};F mice. To better
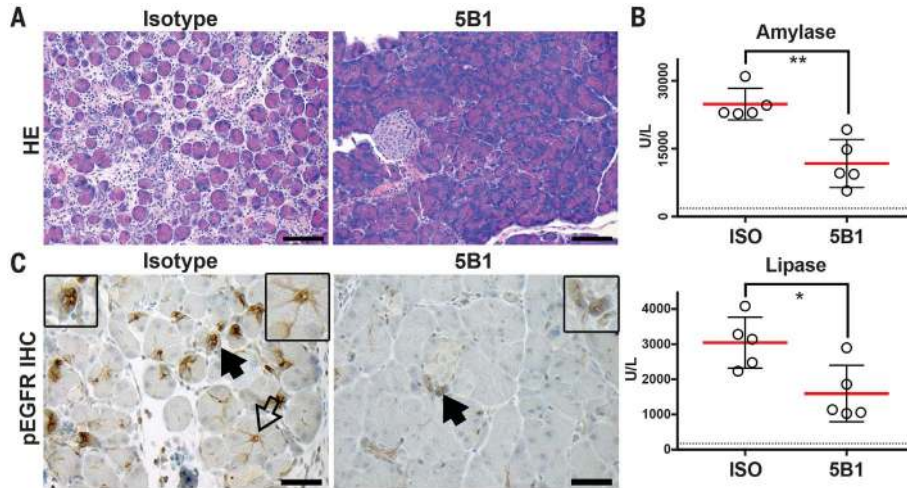
Fig. 5. CA19-9 as a therapeutic target for the treatment of pancreatitis. (**A**) HE staining of representative areas from C;R^{LSL};F mice after treatment with human isotype control (hIgG1; $n = 5$) or the CA19-9 antibody clone 5B1 ($n = 5$) for 8 days and Dox for the last 7 days. Scale bars = 100 μm. (**B**) Serum amylase and lipase levels in C;R^{LSL};F mice treated with 5B1 or isotype control. (**C**) Phospho-EGFR IHC on representative mice treated with either isotype or 5B1 as described in Fig. 5A. Scale bars = 50 μm. Middle horizontal red lines represent the mean, and error bars represent the standard deviation; each data point represents a measurement from an individual mouse. P value was determined by using an unpaired, parametric, two-tailed t test. *$P < 0.05$, **$P < 0.01$.
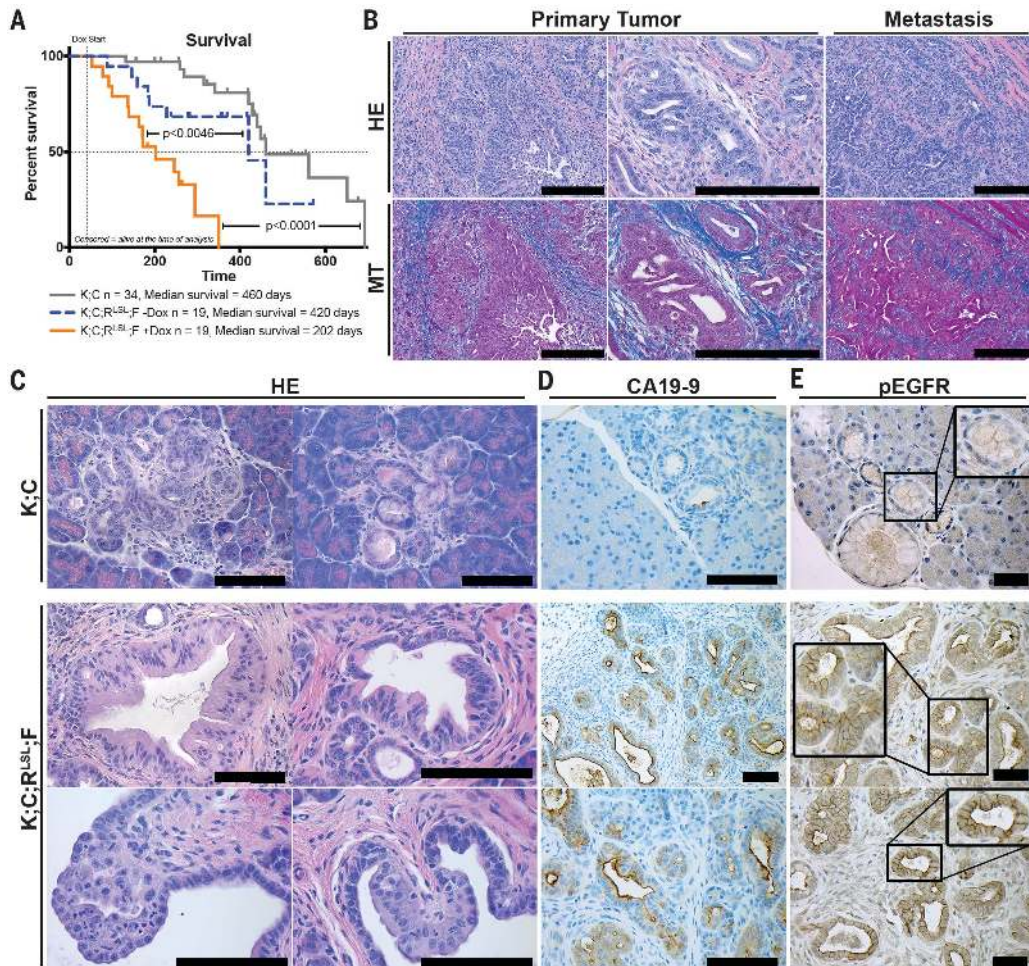
Fig. 6. CA19-9 promotes rapid and aggressive pancreatic tumorigenesis. (**A**) Survival curve for untreated (eight deaths out of 19 mice) and Dox-treated K;C;R^{LSL}:F mice (14 deaths out of 19 mice) and K;C GNs (13 deaths out of 34 mice). The P value was determined by a log-rank Mantel-Cox test. (**B**) Representative histology of pancreatic tumors and metastatic lesions from Dox-treated K;C;R^{LSL}:F mice. Scale bars = 200 μm. (**C**) Representative histology (scale bars = 100 μm), (**D**) CA19-9 IHC (scale bars = 100 μm), and (**E**) pEGFR IHC (scale bars = 50 μm) of the pancreata from K;C and K;C;R^{LSL};F mice after 2 to 4 weeks of Dox treatment.

understand the role of CA19-9 in PDAC initiation, we examined the effect of short-term CA19-9 expression on pancreatic transformation. Whereas littermate controls exhibited the expected low burden of mPanIN-1A lesions, CA19-9–expressing animals harbored a high penetrance of cystic and fibroinflammatory disease with abundant mPanIN-1B and occasional mPanIN-2 lesions after 2 weeks of Dox (Fig. 6C) and increased macrophage infiltration relative to the K;C control cohort (fig. S24, B and C). After 4 weeks of Dox, cystic papillary neoplasia and invasive carcinoma could be detected (Fig. 6C). CA19-9 expression was elevated in normal, benign-reactive, and metaplastic ducts as well as in mPanIN and PDAC lesions in K;C;R^{LSL};F mice, similar to the human expression pattern (Fig. 6D and fig. S12). Equivalent levels of CA19-9 were also observed in human PDAC and mouse K;C;R^{LSL};F organoids (fig. S24D). Phosphorylated EGFR (Fig. 6E) was detected at high levels in Dox-treated K;C;R^{LSL};F mice, whereas CA19-9–negative K;C mice exhibited low to negative levels of phospho-EGFR.

Discussion

CA19-9 is expressed at low levels in the normal ducts of the pancreas but becomes elevated in benign-reactive, metaplastic, and malignant ducts in humans. It is conceivable that the degree of CA19-9 elevation could impart a way to control the degree of fibroinflammatory response in both pancreatitis and PDAC. Mice retain the ability to respond to elevations in CA19-9 despite the fact that they do not normally express this glycan. The ability of mice to respond to CA19-9 elevation may be due to the existence of similar regulatory mechanisms for related Lewis antigens (e.g., sialyl-Lewis^x) that are involved in similar processes in other organs and have also been shown to substitute for CA19-9 in individuals lacking this glycan (49).

Patients with pancreatitis have an elevated risk (2.7- to 16.5-fold) of developing PDAC, and individuals with hereditary pancreatitis have a 40 to 55% lifetime risk of developing pancreatic cancer (1, 5). Therapeutic options for pancreatitis patients are now focused on treating the symptoms, and little can be done to facilitate the resolution of idiopathic pancreatitis or to prevent its recurrence, highlighting the need for new treatments. Prophylactic intervention could also be beneficial in the setting of recurrent or hereditary pancreatitis and after certain routine procedures for which pancreatitis is a common outcome. For example, 3.5% of the >700,000 patients undergoing endoscopic retrograde cholangiopancreatography each year in the United States will develop pancreatitis (50, 51); several risk factors can be used to identify patients at elevated risk for endoscopic retrograde cholangiopancreatography–associated pancreatitis (40%) (52). Fully human CA19-9 antibodies have passed phase 1A clinical trials for positron emission tomography imaging of pancreatic cancer (53). This could potentially facilitate rapid translation of CA19-9–targeted therapy to the clinic for the treatment of pancreatitis.

REFERENCES AND NOTES

1. D. Yadav, A. B. Lowenfels, *Gastroenterology* 144, 1252–1261 (2013).
2. C. E. Forsmark, S. S. Vege, C. M. Wilcox, *N. Engl. J. Med.* 375, 1972–1981 (2016).
3. J.-L. Frossard, M. L. Steer, C. M. Pastor, *Lancet* 371, 143–152 (2008).
4. S. E. van Brummelen, N. G. Venneman, K. J. van Erpecum, G. P. VanBerge-Henegouwen, *Scand. J. Gastroenterol. Suppl.* 38, 117–122 (2003).
5. A. B. Lowenfels et al., *N. Engl. J. Med.* 328, 1433–1437 (1993).
6. C. Guerra et al., *Cancer Cell* 11, 291–302 (2007).
7. Y. Zhang et al., *Int. J. Clin. Exp. Med.* 8, 11683–11691 (2015).
8. C. Haglund, J. Lindgren, P. J. Roberts, S. Nordling, *Br. J. Cancer* 53, 189–195 (1986).
9. J. Makovitzky, *Virchows Arch. B* 51, 535–544 (1986).
10. S. H. Itzkowitz et al., *Cancer Res.* 48, 3834–3842 (1988).
11. K. Iwase et al., *Gastroenterology* 91, 576–580 (1986).
12. A. Malesci et al., *Gastroenterology* 92, 60–67 (1987).
13. F. Safi et al., *Pancreas* 2, 398–403 (1987).
14. W. M. Steinberg et al., *Gastroenterology* 90, 343–349 (1986).
15. S. S. Pinho, C. A. Reis, *Nat. Rev. Cancer* 15, 540–555 (2015).
16. M. Thomsen et al., *Br. J. Cancer* 118, 1609–1616 (2018).
17. C. Shi, N. Merchant, G. Newsome, D. M. Goldenberg, D. V. Gold, *Arch. Pathol. Lab. Med.* 138, 220–228 (2014).
18. B. Xia, C. L. Feasley, G. P. Sachdev, D. F. Smith, R. D. Cummings, *Anal. Biochem.* 387, 162–170 (2009).
19. H. Narimatsu, in *Handbook of Glycosyltransferases and Related Genes*, N. Taniguchi, K. Honke, M. Fukuda, Eds. (Springer Japan, 2002), pp. 218–225.
20. N. Ishijima et al., *J. Biol. Chem.* 286, 25256–25264 (2011).
21. S. Sperandio, C. A. Gleissner, K. Ley, *Immunol. Rev.* 230, 97–113 (2009).
22. T. Yue et al., *PLOS ONE* 6, e29180 (2011).
23. T. Yue et al., *Proteomics* 11, 3665–3674 (2011).
24. Y. Hirao, S. Ogasawara, A. Togayachi, *J. Mol. Biomark. Diagn.* 2, 124 (2012).
25. L. E. Dow et al., *PLOS ONE* 9, e95236 (2014).
26. C. Beard, K. Hochedlinger, K. Plath, A. Wutz, R. Jaenisch, *Genesis* 44, 23–28 (2006).
27. D. C. Whitcomb et al., *Pancreatology* 16, 218–224 (2016).
28. A. Takada et al., *Biochem. Biophys. Res. Commun.* 179, 713–719 (1991).
29. A. Takada et al., *Cancer Res.* 53, 354–361 (1993).
30. S. Majumder, S. T. Chari, *Lancet* 387, 1957–1966 (2016).
31. M. R. Struyvenberg, C. R. Martin, S. D. Freedman, *BMC Med.* 15, 29 (2017).
32. P. G. Falk, L. Bry, J. Holgersson, J. I. Gordon, *Proc. Natl. Acad. Sci. U.S.A.* 92, 1515–1519 (1995).
33. A. Habtezion, *Curr. Opin. Gastroenterol.* 31, 395–399 (2015).
34. K. S. Inman, A. A. Francis, N. R. Murray, *World J. Gastroenterol.* 20, 11160–11181 (2014).
35. G. Klöppel, N. V. Adsay, *Arch. Pathol. Lab. Med.* 133, 382–387 (2009).
36. C. M. Ardito et al., *Cancer Cell* 22, 304–317 (2012).
37. C. Navas et al., *Cancer Cell* 22, 318–330 (2012).
38. S. F. Boj et al., *Cell* 160, 324–338 (2015).
39. H. Tiriac et al., *Cancer Discov.* 8, 1112–1129 (2018).
40. A. V. Vieira, C. Lamaze, S. L. Schmid, *Science* 274, 2086–2089 (1996).
41. H. M. Bill et al., *Mol. Cell. Biol.* 24, 8586–8599 (2004).
42. F. Wang et al., *Proc. Natl. Acad. Sci. U.S.A.* 95, 14821–14826 (1998).
43. Y. C. Liu et al., *Proc. Natl. Acad. Sci. U.S.A.* 108, 11332–11337 (2011).
44. K. Matsumoto et al., *Cancer Sci.* 99, 1611–1617 (2008).
45. P. Camaj et al., *Biol. Chem.* 390, 1293–1302 (2009).
46. E. P. Sandgren, N. C. Luetteke, R. D. Palmiter, R. L. Brinster, D. C. Lee, *Cell* 61, 1121–1135 (1990).
47. E. L. Jackson et al., *Genes Dev.* 15, 3243–3248 (2001).
48. S. R. Hingorani et al., *Cancer Cell* 4, 437–450 (2003).
49. H. Tang et al., *Mol. Cell. Proteomics* 14, 1323–1333 (2015).
50. B. J. Elmunzer, Prevention of ERCP-induced pancreatitis. *Pancreapedia: The Exocrine Pancreas Knowledge Base* (2015).
51. P. J. Parekh, R. Majithia, S. K. Sikka, T. H. Baron, *Mayo Clin. Proc.* 92, 434–448 (2017).
52. M. L. Freeman et al., *N. Engl. J. Med.* 335, 909–918 (1996).
53. R. Sawada et al., *Clin. Cancer Res.* 17, 1024–1032 (2011).
54. J. A. Vizcaíno et al., *Nucleic Acids Res.* 44, 11033 (2016).
55. R. Edgar, M. Domrachev, A. E. Lash, *Nucleic Acids Res.* 30, 207–210 (2002).

Science

The glycan CA19-9 promotes pancreatitis and pancreatic cancer in mice

Dannielle D. Engle, Hervé Tiriac, Keith D. Rivera, Arnaud Pommier, Sean Whalen, Tobiloba E. Oni, Brinda Alagesan, Eun Jung Lee, Melissa A. Yao, Matthew S. Lucito, Benjamin Spielman, Brandon Da Silva, Christina Schoepfer, Kevin Wright, Brianna Creighton, Lauren Afinowicz, Kenneth H. Yu, Robert Grützmann, Daniela Aust, Phyllis A. Gimotty, Katherine S. Pollard, Ralph H. Hruban, Michael G. Goggins, Christian Pilarsky, Youngkyu Park, Darryl J. Pappin, Michael A. Hollingsworth and David A. Tuveson

Sweet bystander becomes a villain

Patients with pancreatic cancer often have elevated blood levels of CA19-9, a carbohydrate antigen present on many proteins. CA19-9 is thus commonly used as a biomarker for diagnosing and monitoring disease progression. In a study of mice, Engle *et al.* found that CA19-9 may be more than an innocent bystander that marks the presence of pancreatic disease; it may play a causal role in disease (see the Perspective by Halbrook and Crawford). Transgenic mice expressing the human enzymes that add CA19-9 to proteins developed severe pancreatitis that could be reversed by treatment with CA19-9 antibodies. When the transgenic mice also harbored a *Kras* oncogene, they went on to develop pancreatic cancer. These unexpected observations suggest new avenues for the treatment of pancreatic disease.

Science, this issue p. 1156; see also p. 1132

ARTICLE TOOLS	http://science.sciencemag.org/content/364/6446/1156
SUPPLEMENTARY MATERIALS	http://science.sciencemag.org/content/suppl/2019/06/19/364.6446.1156.DC1
RELATED CONTENT	http://science.sciencemag.org/content/sci/364/6446/1132.full http://stm.sciencemag.org/content/scitransmed/9/391/eaal3226.full http://stm.sciencemag.org/content/scitransmed/9/398/eaah5583.full
REFERENCES	This article cites 68 articles, 15 of which you can access for free http://science.sciencemag.org/content/364/6446/1156#BIBL
PERMISSIONS	http://www.sciencemag.org/help/reprints-and-permissions

Use of this article is subject to the Terms of Service